Erschienen in: Journal of the American Chemical Society : JACS ; 140 (2018), 4. - S. 1305-1312
https://doi.org/10.1021/jacs.7b08975

Control of Chain Walking by Weak Neighboring Group Interactions in Unsymmetrical Catalysts

Laura Falivene,[§,∥] Thomas Wiedemann,[†,∥] Inigo Göttker-Schnetmann,[†] Lucia Caporaso,[*,‡] Luigi Cavallo,[§] and Stefan Mecking[*,†]

[†]Chair of Chemical Materials Science, Department of Chemistry, University of Konstanz, 78464 Konstanz, Germany
[‡]Department of Chemistry, University of Salerno, Via Giovanni Paolo II, 84084 Fisciano (SA), Italy
[§]King Abdullah University of Science and Technology, Chemical and Life Sciences and Engineering, Kaust Catalysis Center, Thuwal 23955-6900, Saudi Arabia

ABSTRACT: A combined theoretical and experimental study shows how weak attractive interactions of a neighboring group can strongly promote chain walking and chain transfer. This accounts for the previously observed very different microstructures obtained in ethylene polymerization by [κ^2-*N*,*O*-{2,6-(3′,5′-$R_2C_6H_3$)$_2$C$_6$H$_3$-N=C(H)-(3,5-X,Y-2-O-C_6H_2)}NiCH$_3$(pyridine)], namely hyperbranched oligomers for remote substituents R = CH_3 versus high-molecular-weight polyethylene for R = CF_3. From a full mechanistic consideration, the alkyl olefin complex with the growing chain *cis* to the salicylaldiminato oxygen donor is identified as the key species. Alternative to ethylene chain growth by insertion in this species, decoordination of the monomer to form a *cis* β-agostic complex provides an entry into branching and chain-transfer pathways. This release of monomer is promoted and made competitive by a weak η^2-coordination of the distal aryl rings to the metal center, operative only for the case of sufficiently electron-rich aryls. This concept for controlling chain walking is underlined by catalysts with other weakly coordinating furan and thiophene motifs, which afford highly branched oligomers with >120 branches per 1000 carbon atoms.

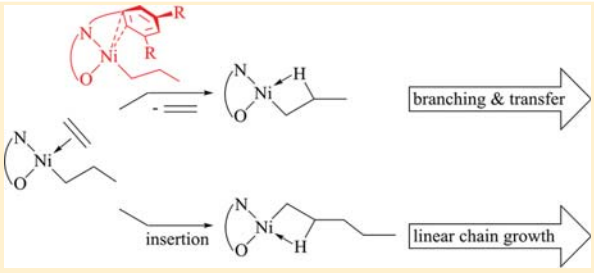

INTRODUCTION

Catalytic insertion reactions promoted by late transition metal complexes are unique in their synthetic and practical scope. Unlike established polyolefin processes,[1,2] they are often tolerant toward heteroatom-containing functional groups, and they provide unique branching structures. A fundamental ubiquitous issue is the occurrence of β-hydride elimination (BHE) in these reactions. In a classical olefin chain growth polymerization, the ratio of insertion chain growth rate vs rate of chain transfer via BHE will determine the products' molecular mass. Moreover, BHE is also a key step of "chain walking", that is, migration of a metal center along a hydrocarbon chain via a series of BHEs and reinsertions.[3−5] This can result in the formation of highly branched polymers from ethylene as the sole monomer (Scheme 1). Such "chain-walking" processes are not restricted to olefin polymerizations but also occur in various other instances.[6−14] For example, they are essential to terminal functionalizations from internal double bonds, which are particularly attractive for the valorization of plant oils.[15] The latter example illustrates a situation frequently encountered: an insertion reaction is strongly favored for the linear metal−alkyl even though branched alkyls are also accessible, resulting in a strong preference for the non-branched, linear product. In fact, even for cases of ethylene polymerization to a strictly linear polymer, extensive underlying chain walking occurs.[16−18]

Scheme 1. Synthetic Relevance of Chain-Walking Processes: Oligomerization of Ethylene to Hyperbranched Oligomers

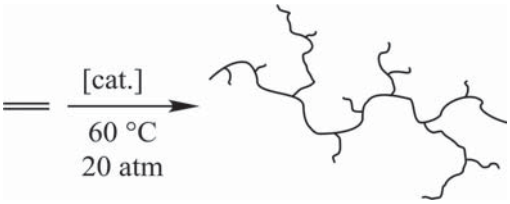

Despite the relevance and utility of chain-walking processes and the underlying step of BHE, a concept is missing to rationally promote or suppress their occurrence and competition with other pathways.

Given this background, neutral nickel(II) salicylaldiminato complexes provide a unique case example. These catalysts, introduced by Grubbs et al.[19] and Johnson et al.,[20] are outstanding in being highly active for ethylene polymerization, stable toward water, and compatible with the presence of certain vinyl monomers.[21−25]

We have advanced these catalysts by introduction of *N*-terphenyl motifs (^{R}**1-pyr**) which allow for an essential tuning of their catalytic properties. This is based on the serendipitous observation that R substituents in an actually rather remote position to the metal site alter the outcome of ethylene polymerization entirely.[26] For example, for R = CF_3 a linear semicrystalline polymer is obtained vs hyperbranched liquid low-molecular-weight oligomers for R = CH_3 (Figure 1). At the same time, the catalysts' stability and activity are very similar.

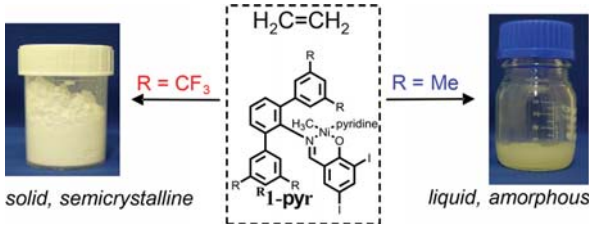

Figure 1. Products of ethylene polymerization depending on the nature of the catalysts' remote substituents R (reaction conditions: 60 °C, 20 atm ethylene pressure).

Due to its practical utility[27−29] and possibly conceptually instructive nature, the origin of this peculiar effect of the remote substituents is being sought.[30−34] Marks and co-workers suggest an attractive F···H interaction of a remote $-CF_3$ group with the growing chain to disfavor BHE,[30] but a fluorine-free electron-withdrawing group yields virtually identical product microstructures.[35] In a related study, the two complexes **2a** and **2b** were

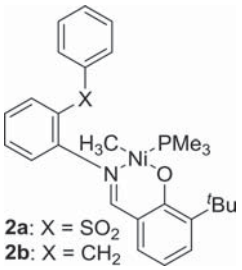

both found to form highly branched ethylene oligomers, with a higher observed activity, 3-fold increased molecular mass, and slightly higher degree of branching for X = SO_2. This is suggested to result from a hemilabile interaction[36−39] of the sulfonyl group.[31] However, the question for a conclusive mechanistic scenario that accounts for increased molecular masses (favored by suppressed BHE) and similar or slightly increased branching (favored by increased BHE) remains open.

Our interpretation from studies of a range of substitution patterns[35−41] is that the electron-withdrawing or -donating nature of the remote substituent (R) is the decisive feature in ^{R}**1-pyr**. However, this is a purely phenomenological account to date.

Overall the underlying mechanisms are not understood.

We now develop a conclusive picture from a comprehensive combined theoretical and experimental study, which shows how weak interactions of a neighboring group can direct the competition between chain growth and BHE.

RESULTS AND DISCUSSION

Phenomenologically, electron-rich substituents in the 3,5-positions of the *N*-terphenyl moiety of ^{R}**1-pyr** make the nickel center more prone for BHE. This increases chain-walking and chain-transfer reactions, explaining the lower molecular mass oligomers with high degrees of branching produced by these complexes. Regarding the open question how the electronic character of the substituents translates to the nickel center, one possibility is a transfer of electron density via increasing the overall electron density of the conjugated system of the salicylaldiminato ligand. A second scenario comprises discrete interactions of the salicylaldiminato ligand with the nickel center additional to its chelating N,O-coordination, e.g., by direct π-interaction between the ligand aryl moieties and the metal center.

Catalyst Precursors and Pressure Reactor Experiments. With regard to the aforementioned issues, molecular structures of the catalyst precursors can be instructive. These neutral Ni(II) salicylaldiminato complexes are stabilized by a P-, N-, or other donor like trimethylphosphine or pyridine. These often bind relatively strongly, and compared with ethylene complexes as an example of species that occur during catalysis they are more stable (note that concerning activation of the precursors for catalysis, this is overcome by the large excess of olefin and the high dilution under pressure reactor conditions). This will alter the role of any additional weak interactions in the catalyst precursor and likely reduce their relevance. For related anilinotropone complexes, Jenkins and Brookhart were able to observe β-agostic complexes at low temperatures.[42] These are devoid of such additional strongly coordinating ligands. Applying analogous synthetic methodology to salicylaldiminato complexes to date did not yield clean, well-characterized products.[43]

Notwithstanding, X-ray diffraction analyses of *N*-terphenyl salicylaldiminato nickel pyridine complexes show that in the solid-state structures, one of the distal aryl rings of the terphenyl moiety is located close to an axial position of the nickel center with typical nickel-aryl distances in the range of 3.05−3.47 Å (Figure 2), the shorter distances being found for

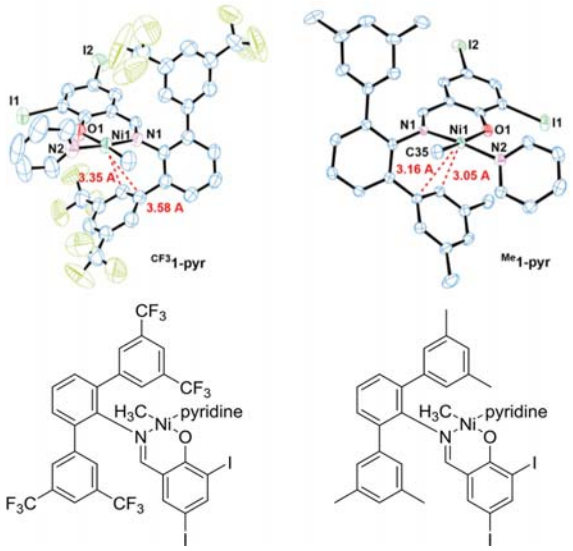

Figure 2. Comparison of X-ray crystal structures (50% probability ellipsoids, H atoms omitted for clarity) of ^{CF3}**1-pyr** and ^{Me}**1-pyr**.

^{Me}**1-pyr**.[26,40,41] These values suggest the possibility of a π-interaction of an aromatic ring with the metal center in this class of complexes.[44]

To further probe for the role of such possible π-interactions, we prepared complexes **3-pyr** and **4-pyr** with electron-rich furanyl and thiophenyl distal aryl motifs. In pressure reactor

Table 1. Polymerization Results with Complexes Bearing Potential Coordinating Motifs in the Ligand Backbone[a]

					M_n [g mol^{-1}]			
entry	catalyst precursor	T [°C]	yield [g]	TOF[b]	NMR[c]	GPC[d]	M_w/M_n (GPC)[d]	branches/1000 C[e]
1[f]	^{CF3}**1-pyr**	50	23.4	41 800		19 000[f]	5.1	10
2	^{Me}**1-pyr**	40	10.9	19 500	1 300	3 500	1.7	77
3	**3-pyr**	40	9.9	17 700	4 800	5 900	1.9	109
4	**3-pyr**	60	6.2	11 100	2 600	5 100	2.0	115
5	**3-pyr**	80	1.8	3 200	1 200	1 800	2.5	112
6	**4-pyr**	40	2.2	3 900	4 100	8 600	1.7	127
7	**4-pyr**	60	0.3	550	2 200	3 500	1.7	123
8	**2a-pyr**	40	2.1	3 800	1 500	2 200	1.9	124
9[g]	**2a-PMe3**	40	2.8	10 000	1 600	2 800	1.9	145[h]

[a]Reaction conditions: 20 μmol of catalyst in 100 mL of toluene for 1 h at 20 bar of ethylene. [b]TOF × mol [C_2H_4] × mol^{-1} [Ni] h^{-1}. [c]Molecular weights calculated from ^{1}H NMR intensity ratio of unsaturated end groups vs overall integral. [d]In THF vs polystyrene standards. [e]Degree of branching calculated from ^{1}H NMR intensity ratio of methyl groups (corrected for saturated end groups) vs overall integral. [f]Data from ref 26: 40 μmol of catalyst for 30 min at 40 bar, GPC data from high-temperature GPC in trichlorobenzene. [g]Data from ref 31: 10 μmol of catalyst, [Ni(cod)$_2$] as cocatalyst at 8 bar for 40 min. [h]Not corrected for end groups.

experiments, they yield ethylene oligomers with very high degrees of branching (Table 1).

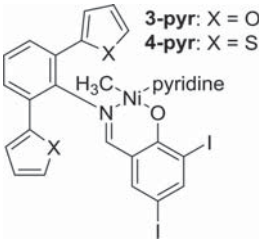

Like for ^{Me}**1-pyr**, the oligomers possess a hyperbranched microstructure as concluded from observable *sec*-Bu branches (cf. Supporting Information (SI)). In detail, degrees of branching exceed those of the terphenyl system (^{Me}**1-pyr**) while molecular weights are slightly higher. Concerning the branching patterns, **3-pyr** and **4-pyr** produce a higher proportion of methyl branches and less higher branches compared to ^{Me}**1-pyr** (Table S1 in the SI). In conclusion, the observed catalytic behavior of complexes **3-pyr** and **4-pyr** underlines that electron-rich potentially coordinating distal substituents promote pathways for branch formation and chain transfer. This is shown here for heteroaromatic rings, going beyond previous findings on substituted phenyl groups.

Cyclic voltammetry on the catalyst precursors showed distinct effects of the nature of the distal aryl rings on the electronic properties of the nickel center. All complexes showed oxidation and reduction transitions during cyclic voltammetry measurements in the potential range expected for a four coordinate square planar Ni(II)/Ni(III) pair. Measurements were carried out using different scan rates from 25 to 2000 mV s^{-1}, and the half-wave potential was found to be independent of the scan rate. The oxidation of all complexes is only partially reversible which is attributed to a relatively fast decomposition of the Ni(III) species. Cyclic voltammograms (cf. Figure S1 in the SI) of the corresponding salicylaldimines did not show any redox transitions at the potentials observed for the complex. Therefore, the oxidation and reduction processes during cyclic voltammetry measurements are assumed to be metal centered. The considerably higher half-wave potential of ^{CF3}**1-pyr** compared to ^{Me}**1-pyr** shows that the nature of the remote substituents clearly affects the electron density at the Ni center, as reflected by the easier oxidation of the more electron-rich ^{Me}**1-pyr** (Table 2). The $E_{1/2}$ values of **3** and **4** are in line with a relatively electron-rich nature.

Table 2. Half-Wave Potentials of Catalyst Precursors According to Cyclic Voltammetry Measurements

entry	complex	$E_{1/2}$ [mV][a]
1	^{CF3}**1-Pyr**	306
2	^{Me}**1-Pyr**	−33
3	**3-Pyr**	84
4	**4-Pyr**	76

[a]Determined from referenced cyclic voltammograms.

An increased electron density at the metal center is expected to result in an increased propensity for BHE and resulting chain transfer. Indeed, molecular masses of the oligomers obtained with the different catalyst precursors and their half-wave potentials decrease from ^{CF3}**1-pyr** > **3** ≈ **4** > ^{Me}**1-pyr**. Regarding degrees of branching of the polymers and oligomers, ^{CF3}**1-pyr** stands out with its low degree of branching and low electron density as reflected by its high $E_{1/2}$ value. For the more electron-rich catalysts ^{Me}**1-pyr**, **3-pyr**, and **4-pyr**, which all yield highly branched oligomers, there is no clear correlation. Degrees of branching are not only governed by the propensity of the catalyst for BHE, but also its relative ability for insertion into a linear alkyl vs different branched alkyls (vide infra). Thus, it appears reasonable that sterics might have a different (higher) impact on chain transfer and add to the effect of electron density at the metal.

These findings show that the nature or substitution pattern, respectively, of the distal aryl rings clearly affects the electronic situation at the metal site as reflected by its redox properties, without implications on how this effect originates.

Active Species and Intermediates during Catalysis. The role of the distal aryl substituents in catalysis was accessed by a comprehensive theoretical DFT study. The reported free energies were built through solvent single point energy calculations on the BP86/6-31G geometries using the M06 functional and the triple-ζ TZVP with the Gaussian09 package. For more details see the SI.

To have a better understanding of the impact of fluorines on the electronic structure of the catalysts, first we analyzed the potential π-interaction between one of the aryl rings of the terphenyl moiety and the nickel center, suggested on the base of the short nickel-aryl distances in the X-ray structure of ^{Me}**1-pyr**. To this end we performed a non-covalent interaction (NCI) analysis using the approach developed by W. Yang and co-workers.[45,46] The gradient isosurface of the reduced density gradient (s = 0.5 au) for ^{Me}**1-pyr**

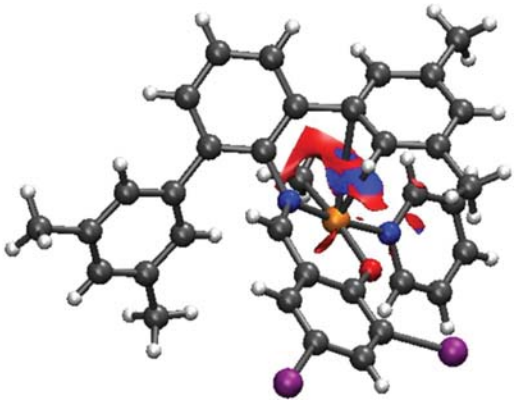

Figure 3. NCI analysis of the electron density of ^{Me}**1-pyr**. The isosurface corresponds to a reduced density gradient isosurface of $s = 0.5$ au The surface is colored on a blue-to-red scale according to the sign of $(\lambda_2)\rho$, ranging from −0.3 to 0.3 au (see the SI for details). Within this scale blue indicates weak attractive interactions, and red indicates weak repulsive interactions. For an additional perspective of the map see Figure S4.

(Figure 3) indicates weak attractive interactions (blue, $\rho = 0.02$ au) along the axis connecting the Ni atom and the vicinal C atoms of the aryl ring, confirming an attractive interaction between the Ni center and the aryl ring of the terphenyl ligand.

To explore whether this interaction can be more relevant during catalysis, when a vacant coordination site can be present on the nickel, we analyzed the coordinatively unsaturated nickel-methyl fragment ^{Me}**1** and ^{CF3}**1** (that is the product of pyridine dissociation from ^{Me}**1-pyr** and ^{CF3}**1-pyr**). For both systems two different isomers were located (Figure 4), one of them showing a

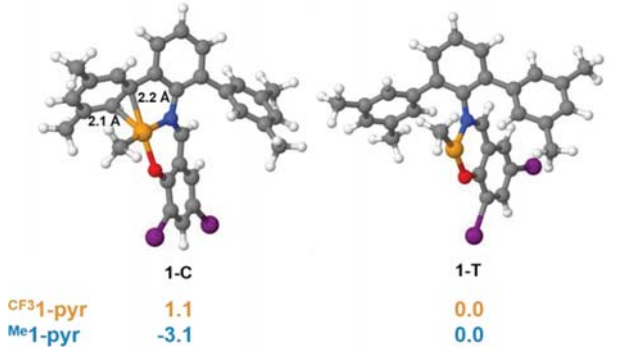

Figure 4. Two possible isomers of the dissociated three-coordinate nickel-methyl species ^{Me}**1** and their relative G_{Tol} in kcal mol^{-1} (G_{Tol} for ^{CF3}**1** isomers are also given).

clear η^2-interaction of one of the distal aromatic rings of the terphenyl moiety of the ligand to the metal center (Figure 4, left).

Notably, for ^{Me}**1** the isomer featuring the η^2-interaction of the aryl ring of the terphenyl moiety (Figure 4, left) is preferred by 3.1 kcal mol^{-1}, whereas for ^{CF3}**1** the isomer having no nickel-aryl η^2-interaction, and having the methyl group trans to oxygen atom is favored by 1.1 kcal mol^{-1} (Figure 4, right). This difference is of course related to the different coordinating ability of the aryl group in ^{Me}**1-pyr** and ^{CF3}**1-pyr** and provides a first indication of a non-covalent interaction possibly relevant during catalysis,[47] which could account for the different catalytic behavior observed for ^{Me}**1-pyr** and ^{CF3}**1-pyr**.

Linear Chain Growth. Starting from **1-*β*-T** (referenced as the zero energy point, Figure 5), ethylene coordination occurring

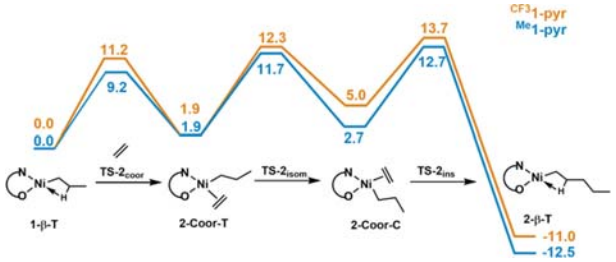

Figure 5. Energy profile (ΔG_{Tol} in kcal mol^{-1}) for the ethylene insertion with complexes ^{Me}**1-pyr** (blue) and ^{CF3}**1-pyr** (orange). Energies are relative to the *β*-agostic *trans*-polymeryl nickel complex **1-*β*-T**.

by opening of the *β*-agostic interaction requires overcoming a free energy barrier of 11.2 (^{CF3}**1**) and 9.2 (^{Me}**1**) kcal mol^{-1}. For both complexes the resulting **2-Coor-T** intermediate is slightly higher in energy relative to **1-*β*-T** + C_2H_4 ($\Delta G = 1.9$ kcal mol^{-1}). Due to the higher energy for the direct ethylene insertion from the **2-Coor-T** intermediate (almost +4 kcal mol^{-1} respect to the insertion from **2-Coor-C**), we investigated the systems' isomerization to the slightly more energetic **2-Coor-C** intermediate via the tetrahedral four-coordinated transition state **TS-2$_{isom}$**. Migratory insertion via **TS-2$_{ins}$** yields the stable *β*-agostic complex, **2-*β*-T**. The overall free energy barrier from **1-*β*-T** to **TS-2$_{ins}$** amounts to 12.7 and 13.7 kcal mol^{-1} for ^{Me}**1** and ^{CF3}**1**, respectively.

The two systems behave similarly in the linear chain growth step, with ^{CF3}**1** showing only a slightly higher energy profile, probably due to a slightly higher steric hindrance in ^{CF3}**1**, as evidenced by topographic steric maps (Figure 6). The main steric hindrance is located in the eastern hemisphere,[48] hosting the monomer in the

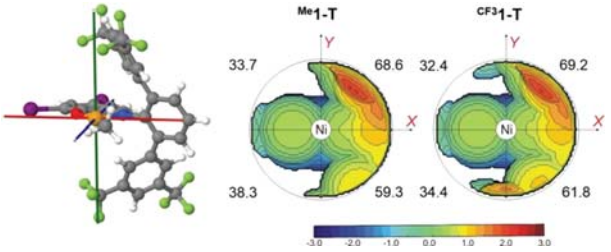

Figure 6. Topographic steric maps of the fragments ^{Me}**1-T** and ^{CF3}**1-T**. The complexes are oriented as shown for ^{CF3}**1-T** on the left.

insertion transition state **TS-2$_{ins}$**. Slightly higher steric hindrance in ^{CF3}**1** can also be observed near the north and south poles, with the CF_3 groups generating steric hindrance in the western hemisphere.

Branch Formation and Chain-Transfer Reactions. Branch formation via both chain walking and chain transfer proceeds with BHE as the initial step.[49] Starting from **1-*β*-T**, BHE leads to the nickel hydride species **1-BHE-T** with a propene molecule coordinated *trans* to the oxygen atom. Due to the unfavorable kinetics and thermodynamics (see Figure 10 in the last section) this possibility was ruled out for both complexes. Hence, BHE has to occur from the *cis* isomer **1-*β*-C**, leading to the sterically less crowded and energetically favored isomer **1-BHE-C**. However, all potential pathways for a direct *cis*/*trans* isomerization of the *β*-agostic complex were calculated to involve transition states with extremely high free energies and therefore can be ruled out (see SI).

An alternative pathway to reach **1-β-C** is through coordination of ethylene to **1-β-T** followed by isomerization of the ethylene complex **2-Coor-T** to **2-Coor-C**—steps already considered in the linear chain growth reaction of Figure 5—followed by ethylene dissociation from **2-Coor-C**, leading to the β-agostic intermediate **1-β-C**.

We found that release of ethylene from **2-Coor-C** can occur via two pathways, see Figure 7. The most straightforward

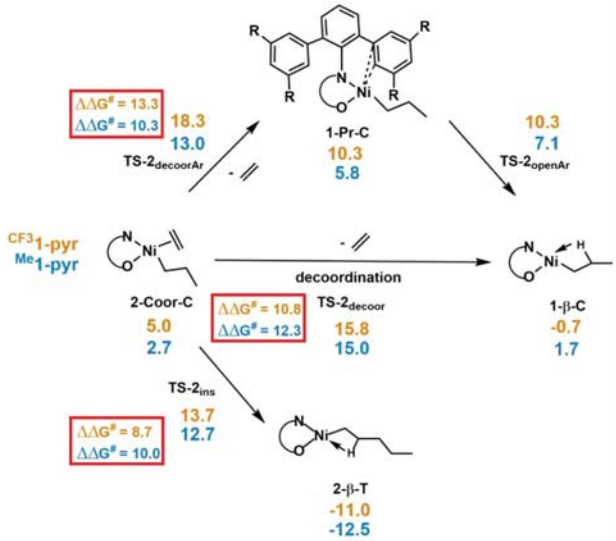

Figure 7. Two potential pathways for the decoordination of ethylene to form **1-β-C**. Free energies (ΔG_{Tol} in kcal mol^{-1}) of all intermediates for ^{Me}**1** (blue) and ^{CF3}**1** (orange).

pathway is direct dissociation of ethylene via **TS-2$_{decoor}$**, with an energy barrier of 12.3 and 10.8 kcal mol^{-1} for ^{Me}**1** and ^{CF3}**1**, respectively. The other ethylene dissociation pathway proceeds in two steps.[50] At first ethylene is displaced by an η^2-interaction of the distal aryl ring of the terphenyl moiety with the Ni center trough **TS-2$_{decoorAr}$**, see Figure 8. In this transition state the

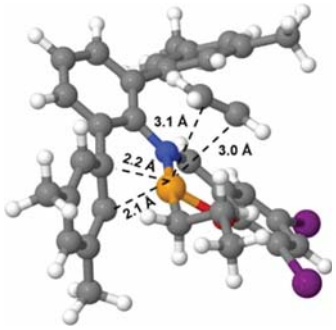

Figure 8. Geometry of TS-2$_{decoorAr}$ for ^{Me}1-pyr system.

complex assumes a square pyramid like geometry with the η^2-interaction of the distal ring lying on the metal plane and the ethylene in the apical position at almost 3 Å from the metal. After displacement of ethylene (i.e., formation of **1−Pr-C**), the ligand-Ni interaction is replaced by a β-agostic hydrogen bond.

As shown in Figure 7, for ^{CF3}**1** the direct pathway is favored by 2.5 kcal mol^{-1} over the two steps pathway (compare barriers of 10.8 and 13.3 kcal mol^{-1} in Figure 7). In contrast, for ^{Me}**1**, the two-step pathway is 2.0 kcal mol^{-1} lower in energy than the direct pathway (compare barriers of 12.3 and 10.3 kcal mol^{-1} in Figure 7). This decisive difference is due to aforementioned stronger interaction between Ni and the electron-rich aryl rings of ^{Me}**1** in the transition state (TS-2$_{decoorAr}$). Hereby, an entry into branching and chain-transfer pathways is enabled (vide infra).

As a result, for ^{Me}**1** formation of **1-β-C** from **2-Coor-C**, with a barrier of 10.3 kcal mol^{-1}, becomes competitive with chain growth from **2-Coor-C**, with a barrier of 10.0 kcal mol^{-1}, by only 0.3 kcal mol^{-1} (Figure 7). Conversely, for ^{CF3}**1**, ethylene insertion from **2-Coor-C**, with a barrier of 8.7 kcal mol^{-1}, is favored by 2.1 kcal mol^{-1} over ethylene dissociation, with a barrier of 10.8 kcal mol^{-1}. The small energy difference between ethylene dissociation and ethylene insertion allows ^{Me}**1** to enter easily into the chain-branching and termination pathways (Figure 9).

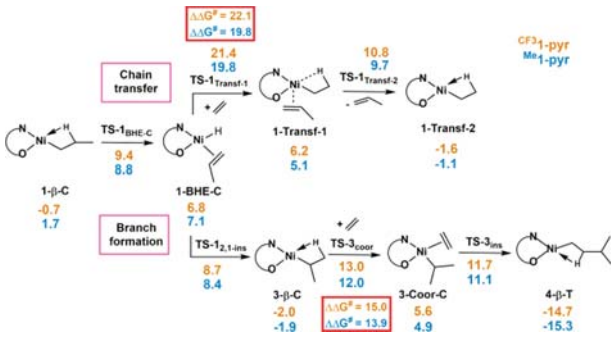

Figure 9. Free energies (ΔG_{Tol} in kcal mol^{-1}) of all important intermediates for chain transfer and branch formation with ^{Me}**1** (blue) and ^{CF3}**1** (orange).

Focusing on ^{Me}**1** energetics, **1-β-C** can undergo BHE with the relatively small barrier of 8.8 kcal mol^{-1} to form the stable **1-BHE-C** intermediate with propene coordinated in the less sterically crowded position. Intermediate **1-BHE-C** can evolve to either chain transfer or chain branching. Chain transfer occurs via coordination and direct insertion of an incoming ethylene molecule via the five-coordinated intermediate **1-Transf-1** and an overall barrier of 19.8 kcal mol^{-1} (Figure 9, top). The following facile release of propene leads to the β-agostic complex **1-Transf-2**, which can start the growth of a new polymer chain.

Moving to the branch formation pathway (Figure 9, bottom), the coordinated propene in **1-BHE-C** can reinsert in a 2,1-fashion via **TS-1$_{2,1\text{-}ins}$**, leading to the β-agostic resting state **3-β-C**. Coordination of a new ethylene molecule displaces the agostic interaction, leading to intermediate **3-Coor-C**. Finally, monomer insertion into the Ni-isopropyl bond via **TS-3$_{ins}$** leads to the methyl branched product **4-β-T**. The rate-determining step along the branch formation pathway is the opening of the agostic interaction by ethylene coordination. According to the numbers reported in Figure 9, for ^{Me}**1-pyr** chain branching is favored over chain termination by 5.9 kcal mol^{-1} (compare barriers of 13.9 and 19.8 kcal mol^{-1} in Figure 9). The overall barrier for branching is only 1.2 kcal mol^{-1} higher than the overall barrier for chain growth (compare barriers of 13.9 and 12.7 kcal mol^{-1} in Figures 9 and 5), which explains the high amount of branching obtained by ^{Me}**1-pyr**.

As for ^{CF3}**1**, both the chain termination and branching pathways are of higher energy compared to the ^{Me}**1** pathways, see Figure 8. Combined with the more difficult access to **1-β-C** calculated for ^{CF3}**1** (Figure 7), this explains the much higher degree of branching of products obtained by ^{Me}**1-pyr** compared to those by

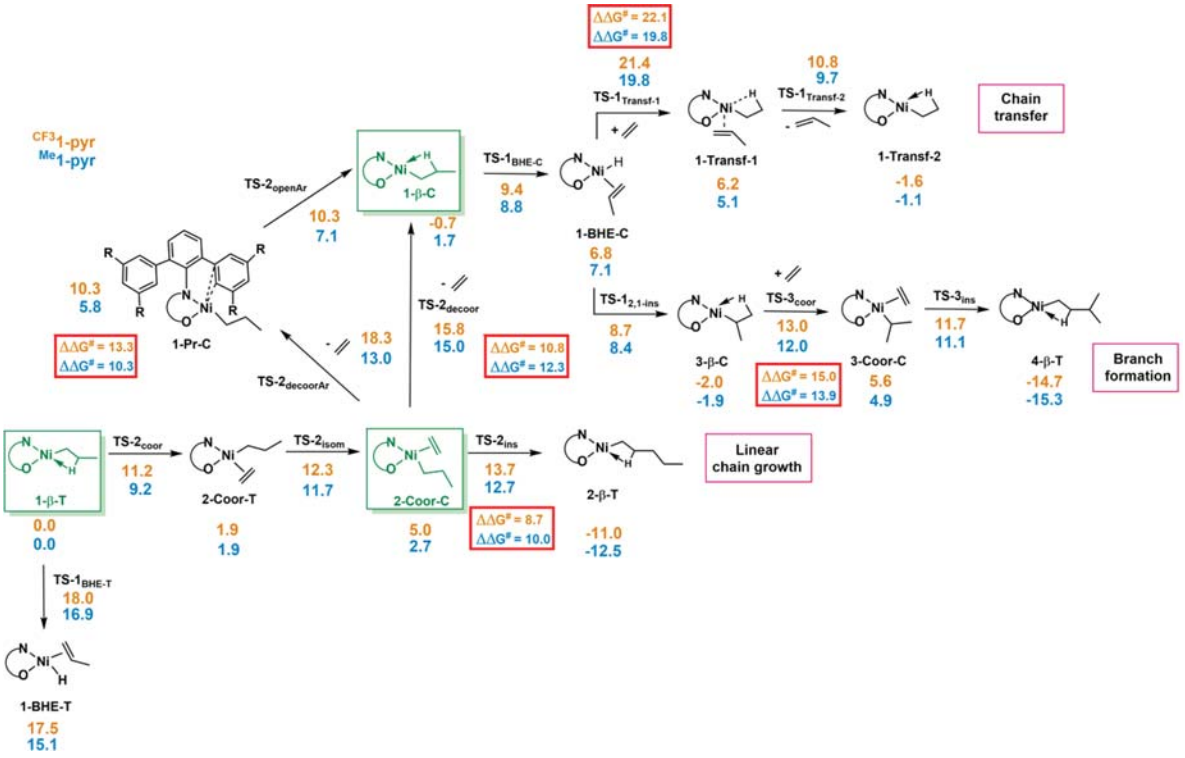

Figure 10. Gibbs free energies (ΔG_{Tol} in kcal mol^{-1}) of all important intermediates for linear chain growth, chain transfer, and branch formation with ^{Me}**1** (blue) and ^{CF3}**1** (orange).

^{CF3}**1-pyr**, and the low-molecular-weight oligomers obtained with ^{Me}**1-pyr** in pressure reactor experiments in contrast to the high-molecular-weight polyethylene produced by ^{CF3}**1-pyr**.

The overall picture emerging (see Figure 10) from DFT calculations indicates that the ethylene complex (**2-Coor-C**), is the key intermediate of the catalytic cycle. It gives access to branch formation and chain-transfer reactions that compete with linear chain growth. This competition affects the product molecular weight and microstructure, i.e., branched or linear products. In line with its decisive role in the catalytic cycle, the largest differences between the two catalytic systems studied are found here. Starting from **2-Coor-C**, for both catalysts linear chain growth has the lowest energy barrier, in agreement with the formation of long chain products including linear sequences (rather than short chain oligomers like butene or hexene). However, for ^{Me}**1-pyr**, branch formation and chain-transfer pathways are accessible with a $\Delta\Delta G^{\ddagger}$ of only 0.3 kcal mol^{-1} relative to the chain growth. This is the result of an energetically favorable pathway involving a weak interaction of the distal aryl ring of the ligand with the metal, which facilitates the releasing of ethylene to form the *cis* β-agostic complex key to chain transfer and branch formation. This pathway is only viable for distal rings with a sufficient coordination ability. Electron-donating substituents promote and enable this pathway, whereas for the case of electron-withdrawing trifluoromethyl groups this pathway is blocked. This results in a distinctively different outcome of the overall catalytic reaction, namely linear polymer vs highly branched oligomers.

As further evidence that energy differences between chain growth vs release of ethylene from **2-Coor-C** to **1-β-C** ($\Delta\Delta G^{\ddagger}_{prop\text{-}elim}$ in kcal mol^{-1}) define the polyethylene microstructure, calculations performed on catalysts analogous to **1** with other remote substituents on the terphenyl distal rings qualitatively agree with their previously found propensity to form highly branched, low-molecular-weight polymers (^{MeO}**1-pyr**) or low-branched linear polymers (^{NO2}**1-pyr**) under pressure reactor conditions (see Table 3).

Table 3. $\Delta\Delta G^{\ddagger}$ as a Measure for the Relative Propensity for Chain Growth Versus Access to Chain-Transfer and Branching Pathways and Experimental Branching

entry	catalyst	$\Delta\Delta G^{\ddagger}_{prop\text{-}elim}$ [kcal mol^{-1}]	branches/1000 C[d]
1[a]	^{CF3}**1-pyr**	−2.1	10
2[b]	^{NO2}**1-pyr**	−1.6	11
3[c]	**3-pyr**	−0.4	109[c]
4[a]	^{Me}**1-pyr**	−0.3	77
5[a]	^{MeO}**1-pyr**	−0.2	79

[a]Taken from ref 26, polymer obtained at 40 bar ethylene, 50 °C. [b]Taken from ref 26, polymer obtained at 40 bar ethylene, 50 °C. [c]This work, polymer obtained at 20 bar ethylene, 40 °C. [d]Determined by ^{13}C NMR spectroscopy.

Finally, for a structurally different catalyst **3-pyr** with terphenyl distal rings replaced by 2-furanyl substituents, the calculated $\Delta\Delta G^{\ddagger}_{prop\text{-}elim}$ = −0.4 kcal mol^{-1} agrees with its experimentally observed ability to form low-molecular-weight highly branched oligomers compared to ^{CF3}**1-pyr** (for complete DFT data cf. SI). Interestingly, the key interaction of the ligand with the metal occurs also in this case through an η^2-coordination of the ring rather than via the lone pair of the furanyl oxygen, as reported in Figure 11 for **1-T**.

CONCLUSIVE SUMMARY

From the combined theoretical and experimental study of reaction pathways during catalysis and complementing experimental

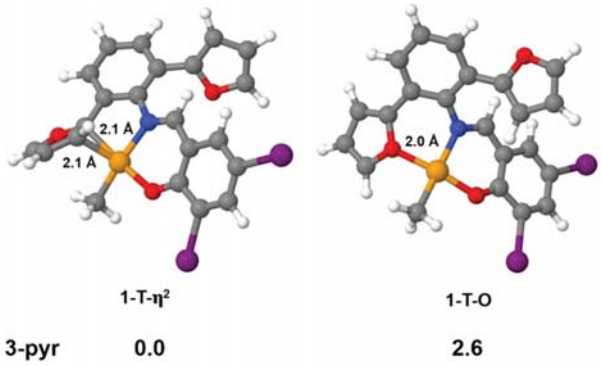

Figure 11. Two possible isomers **1-T** of the dissociated three-coordinate nickel-methyl starting species of catalyst **3-pyr** and their relative G_{Tol} in kcal mol^{-1}.

properties of the catalyst precursors, a conclusive mechanistic account evolves. This reveals an additional weak interaction of a neighboring group as the source of the peculiar effect of the rather remote substituents.

A key underlying element is the unsymmetric nature of the catalysts, with an N,O-coordinating chelating ligand. Chain growth occurs from the alkyl olefin species with the growing chain *cis* to the oxygen donor. Alternative to this chain growth, release of the olefin to the corresponding *cis* β-agostic alkyl can occur. This can undergo facile β-hydride elimination (BHE), which by further reaction steps results in chain transfer or branch formation. It is important to note that the *trans* β-agostic alkyl—which is the product of the aforementioned migratory chain growth event—does not undergo BHE which is associated with a high barrier for this isomer. The olefin release step, which is decisive for the microstructure obtained, can be facilitated by additional weak binding interactions of the chelating N,O-ligand: coordination of the distal aryl rings stabilizes an ethylene-free intermediate, from which the *cis* β-agostic alkyl forms. This pathway is only viable for sufficiently strongly binding motifs, and in the system studied it is not accessible for aromatics that are electron deficient as a result of electron-withdrawing substituents.

These findings explain the formation of very different, useful products in preparative polymerization experiments with these robust and very active catalysts as controlled by the choice of substituents. More generally, they provide a concept for addressing the competition between BHE and chain growth via weak attractive interactions of a specific site of the (chelating) ligand. As BHE is the decisive step for chain walking as well as release of substrate from the catalyst, this applies to polymerization as well as isomerization catalytic reactions.[6−15] Isomerizing functionalization schemes are increasingly developed for the selective generation of complex molecules with biochemical activity. The concept revealed here can contribute to also advancing such synthetic schemes, in addition to controlling polymer materials' properties.

AUTHOR INFORMATION

Corresponding Authors

*lcaporaso@unisa.it

*stefan.mecking@uni-konstanz.de

ORCID

Inigo Göttker-Schnetmann: 0000-0003-1059-9689

Luigi Cavallo: 0000-0002-1398-338X

Stefan Mecking: 0000-0002-6618-6659

Author Contributions

‖L.F. and T.W. contributed equally.

Notes

The authors declare no competing financial interest.

ACKNOWLEDGMENTS

Financial support by the DFG (Me1388/14-1) and by Byk is gratefully acknowledged. Stefano Santacroce, Florian Wimmer, and Giusi Boffa contributed as a part of their undergraduate studies. We thank Rainer Winter for discussions of cyclic voltammetry data.

REFERENCES

(1) Stürzel, M.; Mihan, S.; Mülhaupt, R. *Chem. Rev.* **2016**, *116*, 1398−1433.

(2) Baier, M. C.; Zuideveld, M. A.; Mecking, S. *Angew. Chem., Int. Ed.* **2014**, *53*, 9722−9744.

(3) Johnson, L. K.; Killian, C. M.; Brookhart, M. *J. Am. Chem. Soc.* **1995**, *117*, 6414−6415.

(4) Moehring, V. M.; Fink, G. *Angew. Chem., Int. Ed. Engl.* **1985**, *24*, 1001−1003.

(5) Guo, L.; Dai, S.; Sui, X.; Chen, C. *ACS Catal.* **2016**, *6*, 428−441.

(6) Wakamatsu, H.; Nishida, M.; Adachi, N.; Mori, M. *J. Org. Chem.* **2000**, *65*, 3966−3970.

(7) Behr, A.; Obst, D.; Westfechtel, A. *Eur. J. Lipid Sci. Technol.* **2005**, *107*, 213−219.

(8) Ghebreyessus, K. Y.; Angelici, R. J. *Organometallics* **2006**, *25*, 3040−3044.

(9) Grotjahn, D. B. *Pure Appl. Chem.* **2010**, *82*, 635−647.

(10) Kochi, T.; Hamasaki, T.; Aoyama, Y.; Kawasaki, J.; Kakiuchi, F. *J. Am. Chem. Soc.* **2012**, *134*, 16544−16547.

(11) Werner, E. W.; Mei, T.-S.; Burckle, A. J.; Sigman, M. S. *Science* **2012**, *338*, 1455−1458.

(12) Zhang, C.; Santiago, C. B.; Kou, L.; Sigman, M. S. *J. Am. Chem. Soc.* **2015**, *137*, 7290−7293.

(13) Juliá-Hernandez, F.; Moragas, T.; Cornella, J.; Martin, R. *Nature* **2017**, *545*, 84−89.

(14) Lin, L.; Romano, C.; Mazet, C. *J. Am. Chem. Soc.* **2016**, *138*, 10344−10350.

(15) Goldbach, V.; Roesle, P.; Mecking, S. *ACS Catal.* **2015**, *5*, 5951−5972.

(16) Kanazawa, M.; Ito, S.; Nozaki, K. *Organometallics* **2011**, *30*, 6049−6052.

(17) Conley, M. P.; Jordan, R. F. *Angew. Chem., Int. Ed.* **2011**, *50*, 3744−3746.

(18) Noda, S.; Nakamura, A.; Kochi, T.; Chung, L. W.; Morokuma, K.; Nozaki, K. *J. Am. Chem. Soc.* **2009**, *131*, 14088−14100.

(19) Younkin, T. R.; Connor, E. F.; Henderson, J. I.; Friedrich, S. K.; Grubbs, R. H.; Bansleben, D. A. *Science* **2000**, *287*, 460−462.

(20) Johnson, L. K.; Bennett, A. M. A.; Ittel, S. D.; Wang, L.; Parthasarathy, A.; Hauptman, E.; Simpson, R. D.; Feldman, J.; Coughlin, E. B. (DuPont). Eur. Pat. EP952997B1, 2004.

(21) Mu, H.; Pan, L.; Song, D.; Li, Y. *Chem. Rev.* **2015**, *115*, 12091−12137.
(22) Leblanc, A.; Grau, E.; Broyer, J.-P.; Boisson, C.; Spitz, R.; Monteil, V. *Macromolecules* **2011**, *44*, 3293−3301.
(23) Radlauer, M. R.; Buckley, A. K.; Henling, L. M.; Agapie, T. *J. Am. Chem. Soc.* **2013**, *135*, 3784−3787.
(24) Xi, Z.; Bazzi, H. S.; Gladysz, J. *J. Am. Chem. Soc.* **2015**, *137*, 10930−10933.
(25) Ölscher, F.; Göttker-Schnetmann, I.; Monteil, V.; Mecking, S. *J. Am. Chem. Soc.* **2015**, *137*, 14819−14828.
(26) Zuideveld, M. A.; Wehrmann, P.; Röhr, C.; Mecking, S. *Angew. Chem., Int. Ed.* **2004**, *43*, 869−873.
(27) Osichow, A.; Rabe, C.; Vogtt, K.; Narayanan, T.; Harnau, L.; Drechsler, M.; Ballauff, M.; Mecking, S. *J. Am. Chem. Soc.* **2013**, *135*, 11645−11650.
(28) Wiedemann, T.; Voit, G.; Tchernook, A.; Roesle, P.; Göttker-Schnetmann, I.; Mecking, S. *J. Am. Chem. Soc.* **2014**, *136*, 2078−2085.
(29) Wiedemann, T.; Tchernook, A.; Göttker-Schnetmann, I.; Mecking, S.; Bessel, M.; Omeis, J.; Frank, A. (Byk-Chemie GmbH). Eur. Pat. EP2891511A1, Nov 22, 2013.
(30) Weberski, M. P.; Chen, C.; Delferro, M.; Zuccaccia, C.; Macchioni, A.; Marks, T. J. *Organometallics* **2012**, *31*, 3773−3789.
(31) Stephenson, C. J.; McInnis, J. P.; Chen, C.; Weberski, M. P.; Motta, A.; Delferro, M.; Marks, T. J. *ACS Catal.* **2014**, *4*, 999−1003.
(32) Wang, J.; Yao, E.; Chen, Z.; Ma, Y. *Macromolecules* **2015**, *48*, 5504−5510.
(33) Hu, Y.; Dai, S.; Chen, C. *Dalton Trans.* **2016**, *45*, 1496−1503.
(34) Chen, Z.; Mesgar, M.; White, P. S.; Daugulis, O.; Brookhart, M. *ACS Catal.* **2015**, *5*, 631−636.
(35) Osichow, A.; Göttker-Schnetmann, I.; Mecking, S. *Organometallics* **2013**, *32*, 5239−5242.
(36) Jeffrey, J. C.; Rauchfuss, T. B. *Inorg. Chem.* **1979**, *18*, 2658−2666.
(37) Mecking, S.; Keim, W. *Organometallics* **1996**, *15*, 2650−2656.
(38) Bader, A.; Lindner, E. *Coord. Chem. Rev.* **1991**, *108*, 27−110.
(39) Slone, C. S.; Weinberger, D. A.; Mirkin, C. A. The Transition Metal Coordination Chemistry of Hemilabile Ligands. In *Progress in Inorganic Chemistry*; John Wiley & Sons, Inc.: New York, 2007; pp 233−350.
(40) Göttker-Schnetmann, I.; Wehrmann, P.; Rohr, C.; Mecking, S. *Organometallics* **2007**, *26*, 2348−2362.
(41) Bastero, A.; Göttker-Schnetmann, I.; Röhr, C.; Mecking, S. *Adv. Synth. Catal.* **2007**, *349*, 2307−2316.
(42) Jenkins, J. C.; Brookhart, M. *J. Am. Chem. Soc.* **2004**, *126*, 5827−5842.
(43) Voit, G.; Mecking, S., unpublished results.
(44) In fact, also for **2a** in the solid state, the distal aryl ring is located over the Ni center; cf. ref 31.
(45) Johnson, E. R.; Keinan, S.; Mori-Sánchez, P.; Contreras-García, J.; Cohen, A. J.; Yang, W. *J. Am. Chem. Soc.* **2010**, *132*, 6498−6506.
(46) Contreras-García, J.; Johnson, E. R.; Keinan, S.; Chaudret, R.; Piquemal, J.-P.; Beratan, D. N.; Yang, W. *J. Chem. Theory Comput.* **2011**, *7*, 625−632.
(47) Neel, A. J.; Hilton, M. J.; Sigman, M. S.; Toste, F. D. *Nature* **2017**, *543*, 637−646.
(48) Falivene, L.; Credendino, R.; Poater, A.; Petta, A.; Serra, L.; Oliva, R.; Scarano, V.; Cavallo, L. *Organometallics* **2016**, *35*, 2286−2293.
(49) The chain-transfer reaction involving a monomer-assisted β-hydride elimination is not energetically competitive.
(50) Jian, Z.; Falivene, L.; Boffa, G.; Ortega Sánchez, S.; Caporaso, L.; Grassi, A.; Mecking, S. *Angew. Chem., Int. Ed.* **2016**, *55*, 14378−14383.